Nanosecond fluorescence microscopy

Emission kinetics of Fura-2 in single cells

Susan M. Keating and Theodore G. Wensel
Department of Cell Biology, Sherman Fairchild Building, Stanford University School of Medicine, Stanford, California 94305 USA

ABSTRACT A microscope based time-correlated single photon counting instrument has been constructed to measure fluorescence intensity and emission anisotropy decays from fluorophores in single cells on a nanosecond time scale. The sample is excited and the emission collected using epi-illumination optics with frequency-doubled pulses from the cavity-dumped output of a synchronously pumped dye laser serving as an excitation source. Collection of decays from a single cell is possible due to the presence of an iris in the emission path that can be reduced to less than the diameter of a single cell. Using this instrument the decay of 60 nM 1,6-diphenyl-1,3,5-hexatriene was measured, demonstrating that adequate data for lifetime analysis can be recorded from fewer 10^3 molecules of the fluorophore in an illuminated volume of 23 fl. In addition, the intensity and anisotropy decays of fura-2 in single adherent cells and in suspensions of fura-2 loaded cells were measured for comparison. Data from single cells are in agreement with data obtained with cells in suspension, although the relative amplitudes and decay constants vary somewhat from cell to cell. The results indicate that a significant but variable fraction of fura-2 is bound to relatively immobile macromolecular components in these cells.

INTRODUCTION

Time-resolved fluorescence measurements are frequently used to investigate the mobility and environmental properties of intrinsic or extrinsically added fluorescent molecules and the macromolecules to which the probes are bound. Intensity decays provide information about the fluorophore environment and the heterogeneity of the fluorophore population, while anisotropy measurements provide information about the hydrodynamic properties and segmental flexibility of macromolecules (1–3). The decays of fluorophores in cells can also indicate whether they are free in the cyotoplasm or bound to macromolecules, membranes, or cytoskeletal elements. These measurements typically employ either time (4) or frequency domain (5, 6) methods and solutions or suspensions with observed volumes on the order of cubic millimeters to cubic centimeters. In some cases it may be more useful to measure decays from volumes on the order of a cubic micrometer using a microscope. In a microscope a larger fraction of the total emission can be collected than in a traditional cuvette instrument due to the high numerical aperture of the objective. The emission from a single cell can be measured with reduced interference from the background and scattering problems present in many cuvette measurements of cell suspensions. Moreover, individual variations in the decays from cell to cell can be observed.

Although microscopes are often used to obtain time domain information in the microsecond to millisecond range (7–9), there are only a few reports of nanosecond decays measured with these instruments (10–14). The nanosecond fluorescence microscopes previously reported make use of fast analogue (10, 11), phase modulation (12) and time-correlated single photon counting (13) methods for the measurement of lifetime decays. These instruments have been used only for a few studies of the intensity decays from cell populations and mixtures of model compounds. However, the sensitivity of these nanosecond microscopes, and the range of their applications to single cells have not been explored, particularly in the study of rotational dynamics of intracellular probes.

We have constructed a nanosecond fluorescence microscope to investigate whether fluorescence intensity and anisotropy decays from single, living cells can be measured. The instrument makes use of time-correlated single photon counting methods, including a pulsed laser source, interfaced to a microscope. An important feature of the instrument is the presence of an adjustable diaphragm that can reduce the collected emission to that from a single cell. We have tested the sensitivity

Address correspondence to Dr. Keating.
Dr. Wensel's present address is Department of Biochemistry, Baylor College of Medicine, One Baylor Plaza, Houston, TX 77030.

Abbreviations used in this paper: CPK, creatine phosphokinase; DMP, 1,4-bis(4-methyl-5-phenyl-2-oxazolyl)benzene; DMSO, dimethyl sulfoxide; DPH, 1,6-diphenyl-1,3,5-hexatriene; ETOH, ethanol; EDTA, ethylenediaminetetraacetic acid; EGTA, ethylene glycol-bis(b-aminoethyl ether) *N,N,N′,N′*-tetraacetic acid; NFM, nanosecond fluorescence microscope; NA, numerical aperture.

0006-3495/91/01/186/17 $2.00

of the instrument using 1,6-diphenyl-1,3,5-hexatriene (DPH), and have compared results with this probe as well as with antibody-bound dansyllysine and the Ca^{2+}-indicator dye fura-2, to those obtained in conventional cuvette instruments. The fura-2 measurements were carried out both on the free dye in solution, and within cells. To our knowledge this is the first report of an instrument that can be used to obtain single photon counting intensity and anisotropy data, with good signal-to-noise ratios, from single cells.

Fura-2 (15) is one of the most widely used fluorescent probes for following cellular events in real time. Because the excitation and emission maxima of fura-2 shift from 362 and 512 nm to 335 and 505 nm, respectively, when the dye binds Ca^{2+}, accompanied by an increased quantum yield, this dye has been very useful as a probe of intracellular Ca^{2+} fluctuations. The changes in intracellular free Ca^{2+} are typically monitored by determining the ratio of emission intensities from excitation at 340 and 380 nm. Measurements (16, 17) of translational diffusion coefficients and the steady state anisotropy of fura-2 in muscle fibers has indicated that a substantial fraction of fura-2 may bind to macromolecular components inside muscle cells. Similar effects were observed upon binding to abundant cellular proteins, and such binding was found to alter both the Ca^{2+}-binding affinity and spectral properties of the dye (17). If fura-2 does bind to macromolecules in cells, the time-resolved intensity and anisotropy decay properties of the intracellular form of the probe should be substantially different from those of the free dye. Therefore, we measured the time-resolved decays of fura-2 in single rat basophilic leukemia cells and compared the results to the decays from a suspension of cells measured in a conventional macroscopic pulse instrument, and to those of Ca^{2+}-free and Ca^{2+} bound fura-2 in the presence and absence of high concentrations of protein. Our measurements serve to confirm that fura-2 does in fact bind to large, relatively immobile components in nonmuscle cells as well, and demonstrate that the binding varies from cell to cell within a population of cultured cells.

MATERIALS

Chemicals

Fura-2, pentapotassium salt and AM (eater), as well as DPH were from Molecular Probes (Eugene, OR). Minimal Essential Medium, trypsin-EDTA, fetal calf serum, and gentamicin were from Gibco Laboratories (Grand Island, NY). Mineral oil was from Aldrich Chemical Co. (Milwaukee, WI). Immersion oil, type FF was from R. P. Cargille Laboratories, Inc. (Cedar Grove, NJ). Glycerin for objective immersion was from Carl Zeiss Inc. (Thornwood, NY). All other chemicals, including saponin, creatine phosphokinase (CPK), and aldolase (Type X lyophilized powder from rabbit muscle) were from Sigma Chemical Co. (St. Louis, MO). 1,4-bis(4-methyl-5-phenyl-2-oxazolyl)benzene (DMP) from both Aldrich Chemical Co. and Sigma Chemical Co. was used. Monoclonal anti-dansyl IgG_{2b} antibody was a gift from Dr. Aaron B. Kantor (Stanford University School of Medicine) and had been prepared as previously described (21, 34).

Samples

DMP was dissolved in ethanol to an O.D. of 0.12–0.14 at 355 nm, in a 1-cm cuvette. DPH was dissolved in mineral oil and N_2 was bubbled through the sample. Its concentration was determined by absorbance, using an extinction coefficient of $8.0 \times 10^4\ M^{-1}\ cm^{-1}$ at 348 nm. Background decays from samples containing only mineral oil were substracted from all DPH decays. Microscope samples not containing cells included a small number of phenyl agarose beads for focusing. Background emission from the beads was insignificant. The coverslip and slide were sealed at the edges using Apiezon Grease, Type M (Biddle Instruments, Blue Bell, PA). Immersion oil, or in some cases glycerin, was used between the objective and the coverslip, and emission was collected only from the center of the slide.

Solutions of free fura-2 contained 5–20 μM fura-2 salt in saturating EGTA (0.25–1 mM) or 2 mM $CaCl_2$ in buffer. Samples of fura-2 in the presence of protein contained 32 mg/ml aldolase or 25 mg/ml creatine phosphokinase with fura-2 salt in buffer, and either EGTA or Ca^{2+}. The buffer was 20 mM Hepes, pH 7.4 with 150 mM KCl or 135 mM NaCl, 5 mM KCl. Background decays were measured from identical samples to those containing dye, but without fura-2.

Rat basophilic leukemic cells (RBL-2H3 cells) were grown in minimal essential medium supplemented with 20% fetal calf serum and 10% gentamicin in 95% CO_2/5% O_2 at 37°C. The cells were harvested by treatment with trypsin (0.25% trypsin with 1 mM EDTA) for 7 min, diluted in medium and washed by centrifugation. The pellet was resuspended in medium to a concentration of $\sim 10^6$ cells/ml. For measurements of suspensions of fura-2 loaded cells in a cuvette, 1 μM of fura-2 ester (in DMSO) was added to the suspension of cells for 30 min while rotating at room temperature (23°C), washed three times by centrifugation, and resuspended in buffer (20 mM Hepes, 135 mM NaCl, 5 mM KCl, pH 7.4, with or without 1 mM $MgCl_2$ and 2 mM $CaCl_2$) to a concentration of $\sim 10^6$ cells/ml. The cells were loaded at 23°C to minimize compartmentation of the dye into organelles (18). The effect of permeabilizing the plasma membrane and releasing cytoplasmic dye was tested by addition of saponin at a concentration of 50 μg/ml. At this concentration saponin is reported to permeabilize by forming pores only in the cholesterol-rich plasma membrane and not in internal organelles (19).

For measurements of single cells in the microscope, 0.20 ml of cells suspended in media were pipetted onto a coverslip and allowed to adhere while labeling. The cells were labeled with fura-2 ester at room temperature either for 30 min with 1 μM ester, or for 45 min with 2.5 μM ester. The coverslips were dipped in buffer three times, then inverted onto a slide containing 0.10 ml of buffer. As for all the samples measured in the microscope the coverslips and slides were sealed with grease. We estimate, from permeabilized cell studies in this laboratory, that under our loading conditions the intracellular fura-2 concentration is ~ 100 μM (T. Meyer, Stanford University, personal communication). The response of cells to stimuli has been reported to be independent of the concentration of intracellular fura-2 up to at least 200 μM; and fura-2 has been reported to have no effect on secretion (20). Cells used for background measurements were treated identically except that fura-2 was not added.

All solvents, including immersion oil, showed negligible background fluorescence over the wavelengths measured. All measurements were at 23°C.

INSTRUMENTATION

The time-resolved pulsed-laser fluorescence microscope

The nanosecond fluorescence microscope, shown in Fig. 1, consists of standard pulse instrumentation for excitation and signal processing, interfaced to a microscope. A train of picosecond pulses at 355 nm is obtained as previously described (21, 22) by frequency doubling the 710 nm pulses generated by a synchronously pumped, cavity dumped, DCM dye laser, pumped by a mode-locked argon ion laser. The pulse repetition rate is typically 4 MHz or 800 kHz. The pulses pass through a vertically oriented Glan-Thompson polarizer and filters to discriminate against the undoubled 710 nm light, before entering a modified Zeiss Universal Microscope (Carl Zeiss Inc.). Typically the UV excitation is vertically polarized; however, in some cases a polarization rotator (model 310; Spectra Physics, Mountain View, CA) is placed in front of the M1 mirror producing horizontally polarized UV pulses (both orientations result in horizontally polarized excitation impinging upon the microscope sample).

In the microscope, the beam is reflected by a mirror and a dichroic filter (FT420; Carl Zeiss Inc.) into a 100X Neofluar objective (Carl Zeiss Inc., NA = 1.3, oil immersion), which focuses the beam onto the sample between a quartz coverslip and slide (Heraeus-Amersil, Buford, GA). Using a cavity-dumped 710 nm beam of 22 mW, assuming a doubling efficiency of 1%, and accounting for losses due to filters, mirrors, and the objective, the intensity of the excitation at the microscope stage can be estimated to be on the order of 10 μW or 10^{13} photons s^{-1} over an area of $\sim 10^{-6}$ cm^2. The emission collected by the objective is transmitted through the dichroic mirror, filters, a rotating film polarizer, and an adjustable diaphragm. For the work described here LP420 (for the DPH samples) or LP470 (for the fura-2 samples; Carl Zeiss Inc.) and LS550 (Corion Corp., Holliston, MA) emission filters were used. For measurements of antibody-bound dansyllysine a 380 DCLP dichroic filter (Omega Optical, Brattleboro, VT) was used with LP450 (Carl Zeiss Inc.) and LS550 emission filters. The polarizer is periodically rotated (30 s periods) to detect in turn the parallel, $F_{\parallel}$, or perpendicular, $F_{\perp}$, polarized components of the emission. When the fluorescence from a cell is measured, the diaphragm is adjusted to pass an image just less than the cell diameter (12–15 μm). For solution samples the iris is closed to ~10 μm diam, as measured using a Leitz objective micrometer (E. Leitz, Rockleigh, NJ). A beamsplitter and eyepiece above the iris diaphragm allow observation of the image after the pinhole. Adjustment of the iris to be slightly larger than the image of the focused excitation discriminates against out of focus fluorescence and stray light. Finally the emission is focused into a photomultiplier (R928; Hammamatsu Photonics K. K., Hamamatsu City, Japan) in a cooled housing (Products for Research, Inc., Danvers, MA). In some cases a Carl Zeiss Inc. Ultrafluar objective (100X, 0.85 NA, glycerin immersion) is used. The microscope stage and PMT housing are enclosed in black Lucite boxes.

In the single photon counting electronics the signal is amplified (VV101 amplifier) and discriminated (TC454 constant fraction discriminator, Tennelec, Oak Ridge, TN); then used as the start pulse for the time-to-digital converter (TDC) and histogramming memory (models 4202 and 3588; LeCroy Corp., Chestnut Ridge, NY) interfaced to a computer (AT, IBM, Boca Raton, FL). The stop pulse for the TDC is deflected from the 710 nm cavity dumped pulse train by a pellicle and collected by a trigger photodiode (FND100 EG & G Electro-Optics, Salem, MA) before being processed by the discrimination and delay electronics. Approximately 10^5 counts in the peak channels can be

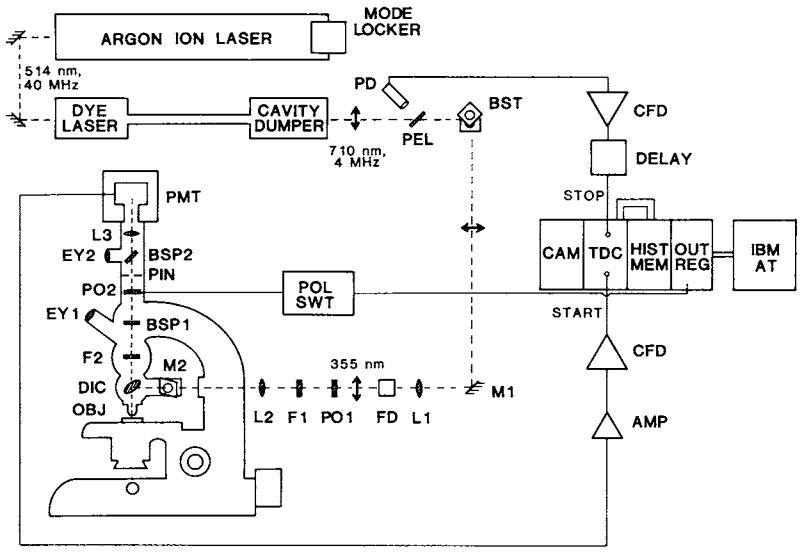

FIGURE 1 Diagram of the nanosecond fluorescence microscope. The dashed line indicates the direction of the light path. The wavelengths and direction of polarization of the laser beam are shown with vertical and horizontal arrows indicating vertical and horizontal polarization, respectively. Abbrevations are: PD, trigger photodiode; PEL, pellicle; BST, beamsteerer; M1-2, mirrors, L1-3, lenses; FD, frequency doubler (KDP crystal); PO1, Glan-Thompson polarizer; F1, excitation filters; OBJ, objective; DIC, dichroic mirror; F2, emission filters; BSP1-2, beamsplitters; EY1-2, eyepieces; PO2, rotating film polarizer; PIN, adjustable iris diaphragm (pinhole); PMT, photomultiplier; AMP, amplifier; CFD, constant fraction discriminator; DELAY, delay lines; CAM, CAMAC crate controller (Kinetic Systems 3920); TDC, time to digital converter; HIST MEM, histogramming memory; OUT REG, output registor for controlling orientation of emission side polarizer; POL SWT, coupled relay, power supply and pneumatic piston for rotating emission side polarizer.

obtained in 10–20 min of data acquisition time. The resolution of the TDC is 0.156 ns/channel. The data is stored and analyzed on the IBM AT.

Standard pulse instrument

The instrument used to measure time-resolved decays from samples in a cuvette has been previously described (21, 22). The frequency doubled laser pulses are in this case directed into this "cuvette" instrument. The data were measured using a LS600 or LS550 and LL450 filter in the emission path (Corion Corp.). The instrument response function is measured using a piece of aluminum foil in the sample compartment to scatter the excitation.

Steady state instrumentation

Fluorescence excitation and emission spectra were measured using an SLM 8000 scanning spectrofluorimeter (SLM Instruments, Inc., Urbana, IL). For the emission spectra the excitation wavelength was 355 nm; for the excitation spectra the emission wavelength was 520 nm. Spectra of cells were measured while stirring.

DATA ANALYSIS

Time-resolved decays

It is often useful to analyze fluorescence intensity and anisotropy decays in terms of simple mono- or biexponential decay laws, characterized by apparent excited state lifetimes τ_i and apparent rotational correlation times ϕ_i. Such analysis requires the deconvolution of the instrument response function from the observed decays, a procedure which is somewhat more difficult in the microscope-based instrument.

The procedure for analysis of the decays measured in the standard cuvette instrument has been previously described (21, 22). The Grinvald-Steinberg deconvolution procedure (23) used involves convolving the instrument response function, measured using a scatterer, with a sum of exponentials to model the true sample decay. In the microscope, the UV excitation is not passed by the optics, so that an instrument response function measured using a scatterer cannot be used. This problem is analogous to those situations in which "color effects" on instrument response kinetics are critical to accurate deconvolution. Therefore, the microscope data have been analzyed using the "delta function convolution" method (24, 25). In this case the decay of a reference measured at the same excitation and emission wavelengths as those used for the sample, and with a known lifetime, is used in the fitting routine. The model to which the data is fit is then a sum of exponentials altered to account for the use of the reference in the fit. A more complete description of the models used for the analysis of the time-resolved data is given in the Appendix.

Both the orthogonal polarization directions that are perpendicular to the direction of propagation of the exciting and the detected light are horizontal (i.e., in the plane of the microscope stage). In the discussion that follows these two directions are referred to as "vertical", denoted by the subscript V, indicating the normal polarization of the excitation pulse which is vertically polarized as it enters the microscope, or "horizontal", denoted by the subscript H, indicating the perpendicular component within the horizontal plane. The nanosecond data from both the cuvette and microscope instruments are collected as the parallel and perpendicular components of the sample emission, F_{SV} and F_{SH}, after excitation with vertically polarized light. In the analysis program the total measured fluorescence intensity, $F_T(t)$, used in the fit is calcualted for both the sample and reference, ($F_{RV}[t]$ and $F_{RH}[t]$), decay by,

$$F_T(t) = F_V(t) + 2F_H(t). \quad (1)$$

In some cases, background decay components $F_{BV}(t)$ and $F_{BH}(t)$ are recorded from samples containing no dye and subtracted from the sample decays. There is no background subtraction for the reference data.

All curve fitting is based on nonlinear least squares procedures using the Marquardt algorithm (26, 27). In the analysis the model decay is calculated using guesses for the component amplitudes, α_i, and the lifetimes, τ_i, and convolved with either the instrument response measured using the scatter, or with the reference data. In all the fits a double exponential model is used to fit the data. The best fit is found by varying the values of the parameters until the weighted sum of the squares of the deviations between the calculated, $F_C(t)$, and the measured, $F_S(t)$, decay is minimized as demonstrated by the value of χ^2.

$$\chi^2 = \Sigma_i\, WF[F_S(t) - F_C(t)]^2, \quad (2)$$

where WF is the weighting factor. The goodness of fit is judged by the value of the reduced χ^2,

$$\chi^2_R = \chi^2/v, \quad (3)$$

where v is the number of degrees of freedom (the difference between the number of data points and the number of floating parameters).

All the data are assumed to obey Poisson statistics. Thus, in the fit of data using a scatterer, the weighting factor is (28):

$$WF = 1/\mathrm{var}F_S(t) = 1/[\mathrm{var}F_{SV}(t) + 4\,\mathrm{var}F_{SH}(t)], \quad (4)$$

where,

$$\mathrm{var}F_{SV}(t) = F_{SV}(t) + F_{BV}(t) \quad (5)$$

and

$$\mathrm{var}F_{SH}(t) = F_{SH}(t) + F_{BH}(t). \quad (6)$$

In the fits where the reference decay is used in the deconvolution procedure, the weighting factor described in Eq. 4, is used in the first pass of the fit, and then *WF* becomes (24),

$$WF = 1/[\mathrm{var}F_S(t) + (\Sigma_i \alpha_i)^2 \mathrm{var}F_R(t)], \quad (7)$$

where $\mathrm{var}F_S(t)$ as is described above and $\mathrm{var}F_R(t)$ is calculated according to Eq. 4, but using the reference data.

The weighted residuals are calculated as,

$$Res = \Sigma_i (WF)^{1/2}[F_S(t) - F_C(t)]. \quad (8)$$

The final values of the parameters returned from the fits are used to calculate the average lifetimes, $\langle\tau\rangle$, and fractional intensities, f_i, according to:

$$\langle\tau\rangle = (\Sigma_i \alpha\tau_i^2)/(\Sigma_i \alpha\tau_i) \quad (9)$$

and

$$f_i = (\alpha_i\tau_i)/(\Sigma_i \alpha_i\tau_i). \quad (10)$$

In the plotting routine the intensity decays are normalized to 10^5 counts.

The anisotropy is calculated from the ratio of the difference of the two polarized components and the total of the sample fluorescence decay,

$$R_S(t) = D_S(t)/F_S(t)$$
$$= [F_{SV}(t) - F_{SH}(t)]/[F_{SV}(t) + 2F_{SH}(t)]. \quad (11)$$

In the analysis of the anisotropy data measured in the cuvette instrument the model is actually fit to the difference curve, $D_S(t)$, as previously described (21, 22). In the deconvolution procedure, the program uses the values for α_i and τ_i from the fit of the intensity, decay, and varies the guesses for the amplitudes, β_i, and the rotational correlation times, ϕ_i, to determine the best fit of the data. A double-exponential decay is used to model the data as discussed in the Appendix. Again, the goodness of fit is judged by the value of the reduced χ^2_R, where,

$$\chi^2 = \Sigma_i WF[D_S(t) - D_C(t)]^2. \quad (12)$$

The weighting factor for the fit of the difference curve is (28):

$$WF = 1/[\mathrm{var}F_{SV}(t) + \mathrm{var}F_{SH}(t)]. \quad (13)$$

The ratio of the calculated difference, $D_C(t)$, and sum, $F_C(t)$ curves, determined from the final parameters of the fit, are used to calculate the anisotropy decay curves in the plotting routine.

Programs have not yet been developed to fit the anisotropy decays using the reference decay and the "delta function convolution" method. The intracellular anisotropy decays are clearly nonexponential, so little information would be gained by attempting to fit them to a biexponential model. However, extension of the deconvolution procedures using the reference to the anisotropy decays should be straightforward.

Calculation of g-factors

The g-factors, which are necessary to correct for any difference in detector sensitivity to emitted light of different polarizations, must be measured differently for epifluorescence than for conventional right-angle instruments. The decay of a sample excited with a vertically polarized pulse contains the parallel and perpendicular components of the emission, F_{VV} and F_{VH}, with horizontally polarized excitation the parallel and perpendicular components are F_{HH} and F_{HV}. If S_V are S_H are the emission detector's sensitivities to vertical and horizontal light, E_V and E_H are the intensities of vertical and horizontal excitation, respectively, M_{VV}, M_{VH}, M_{HH}, and M_{HV} are the *measured* signal intensities corresponding to F_{VV}, F_{VH}, F_{HH}, and F_{HV}, respectively, and $G = S_V/S_H$, then:

$$M_{VV} = E_V S_V F_V \quad (14)$$

$$M_{VH} = E_V S_H F_H \quad (15)$$

$$M_{HH} = E_H S_H F_V \quad (16)$$

$$M_{HV} = E_H S_V F_H \quad (17)$$

so that,

$$M_{VV}/M_{VH} = (S_V F_V)/(S_H F_H) = G(F_V/F_H) \quad (18)$$

and

$$M_{HH}/M_{HV} = (S_H F_V)/(S_V F_H) = (1/G)(F_V/F_H). \quad (19)$$

$$(M_{VV}/M_{VH})/(M_{HH}/M_{HV}) = G^2. \quad (20)$$

To determine the g-factors a series of decays are collected in the microscope from each fluorophore studied, using vertical and horizontal polarization. The intensities in all the time channels were added to give the steady state values, and the summed intensities are then used to calculate G for each sample. The g-factors were found to be 1.0 ($\pm$0.05) in all cases.

High numerical aperture effects

Use of high numerical aperture objectives can lead to distortions of the data as discussed in detail by Axelrod

(29, 30). This is due to the wide angle over which the emission is collected by the objective, which can lead to mixing of the polarization components of the emission. We estimate, using his theory, that for randomly distributed fluorophores, with a numerical aperture of 1.3, the steady state value of anisotropy measured may be depolarized by as much as 25%. In addition, one possible result of these effects is that in time-resolved measurements the calculated total fluorescence will not necessarily represent the total decay and the anisotropy decay will become dependent on τ. To determine the extent of this distortion in our instrument, we compared the decays of samples measured with two 100X objectives with different NA, 1.3 and 0.85.

RESULTS

Tests of Instrument performance

Because the nanosecond fluorescence microscope is a novel instrument we conducted a series of tests of its performance. Decays measured in a conventional time-correlated single photon counting instrument were compared to those measured by NFM including decays from cells. Fig. 2 shows fluorescence and anisotropy decays from fura-2 loaded RBL cells measured in both the nanosecond microscope (single adherent cell) and the conventional pulse instrument (suspension of 10^6 cell/ml). The response of each instrument to the excitation

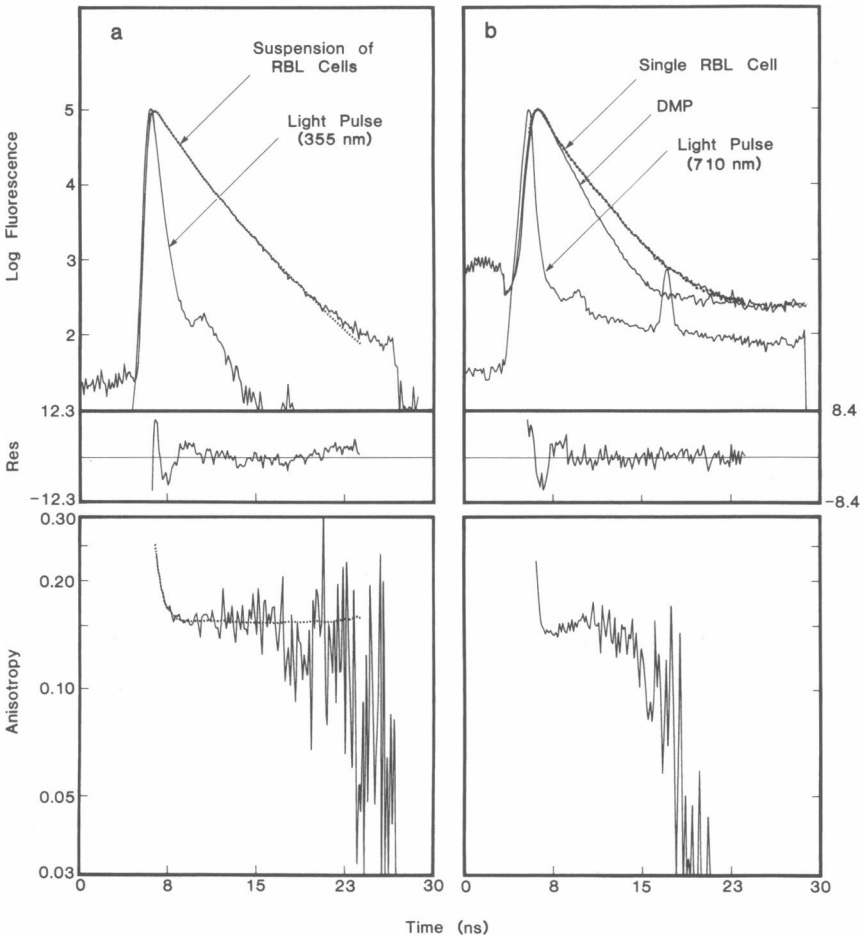

FIGURE 2 Comparison of nanosecond fluorescence decays measured in the cuvette vs. microscope. Fluorescence intensity (*upper panels*) and anisotropy (*lower panels*) decays of fura-2 in RBL cells recorded in *a* the standard cuvette instrument (cell suspension at 10^6 cells/ml) and *b* in the microscope-based instrument (single adherent cell with background from an unlabeled cell subtracted). In *a* the scattered pulse profile, recorded at the excitation wavelength is also shown. Panel *b* shows the pulse profile, containing undoubled excitation (see text) and the decay of the reference fluorophore, DMP in 100% ethanol. The curves from the fits of the data (···) are superimposed on the raw data (—), and are obtained by using either the scattered pulse data (*a*) or the reference decay data (*b*). A two-exponential decay function from the fit of the anisotropy data in *a* is superimposed on the data. No fit is calculated for the anisotropy in *b*. The weighted residuals from the fits are shown in the middle box. The data in *a* was fit over 117 channels, in *b* over 122 channels.

pulse scattered from aluminum foil using UV-passing filters is also shown (*solid lines*). Because the microscope optics effectively filter the exciting light when the scatterer is used, it is actually the small fraction of remaining undoubled (i.e., 710 nm) dye laser emission that is detected, superimposed on any background fluorescence from the instrument and scattering element. To account for the instrument response function accurately, the standard DMP in ethanol is used and its decay curve is also shown. The decay of DMP in ethanol is characterized by a single exponential lifetime of 1.45 ns that is wavelength and temperature invariant (31).

The fits shown superimposed on the intensity data were obtained by reconvolution using the scattered pulse data for the decays measured in the cuvette instrument (*a*), or the DMP decay for the data measured in the microscope (*b*). Comparison of the fits to the raw data, as well as the residual plots (*middle panel,* Fig. 2) and the χ^2 values listed in Table 1 indicate that a somewhat better fit was actually obtained for the microscope data. However, the average lifetimes, $\langle\tau\rangle$, obtained from the fits are similar: 2.06 ns for the suspension of cells and 1.95 ns for the microscope data (cell 3 in Table 1). Analysis of NFM data from 10 different cells loaded in separate experiments on different days, produced $\langle\tau\rangle$ of 1.96 ns ± 0.066 ns (see footnote, Table 1). The typical experimental variability in the NFM measurements, i.e., the range in average lifetimes obtained for the same or similar samples from day to day is approximately ±0.1 ns.

TABLE 1 Fits of time-resolved intensity decays of Fura-2

Conditions	Inst.*	τ_1	f_2	τ_2	$\langle\tau\rangle$	χ^2_R
		ns		*ns*	*ns*	
Ca^{2+}	C	0.532	0.911	1.82	1.71	26.9
$Ca^{2+(B)}$	M	1.92	0.632	1.85	1.88	1.79
EGTA	C	0.633	0.625	1.43	1.13	10.4
$EGTA^{(B)}$	M	0.721	0.722	1.45	1.25	1.74
aldolase, $Ca^{2+(B)}$	C	1.68	0.118	3.20	1.86	20.2
aldolase, $EGTA^{(B)}$	C	1.17	0.309	2.50	1.58	39.8
CPK, EGTA	C	1.18	0.551	2.74	2.04	34.5
RBL cells, intact	C	1.37	0.505	2.74	2.06	8.44
RBL cell $1^{(B)}$	M	0.105	0.869	2.19	1.92	15.2
RBL cell $2^{(B)}$	M	0.751	0.787	2.30	1.97	2.48
RBL cell $3^{(B)}$	M	0.729	0.789	2.27	1.95	4.19
RBL cells, saponin	C	9.72	0.962	2.34	2.62	3.00

*Data measured in the cuvette pulse instrument (*C*) were analyzed using a scatter for the instrument response function; microscope decays (*M*) were fit using the reference decay of DMP. All decays were analyzed using a double-exponential fit. f_2 is the fractional amplitude of component 2.

$\langle\tau\rangle$ is the average lifetime.

$^{(B)}$ indicates that the appropriate background decay was subtracted from the data in the analysis routine.

RBL cell 1 was labeled under different conditions than cells 2 and 3, which are from the same preparation. The decay parameters averaged from the fit of 10 different single cell measurements (under different labeling conditions) are f_1 = 0.182 (±0.057), τ_1 = 0.535 (±0.383) ns, f_2 = 0.818 (±0.057), τ_2 = 2.26 (±0.095) ns and $\langle\tau\rangle$ = 1.96 (±0.066) ns.

The anisotropy decays are also similar, but show more significant differences than the lifetime data. While both decays have both very fast decay components and very slow ones, the single cell NFM decay has a lower initial anisotropy than the cuvette data, displays regions where the anisotropy actually increases with time, and deteriorates into a noisily and rapidly decaying trace at times more than 7 ns after the excitation pulse.

In Fig. 2 a two-exponential decay function from the fit of the anisotropy data in *a* is superimposed on the data. No fit is calculated for *b*. The agreement of the data with the double-exponential fit in *a* does not necessarily indicate that the dye experiences only two environments. In fact, the data below suggest a heterogenous population of fura-2 in the cells, with the various species differing both in fluorescence decay constants and in rotational diffusion constants. The pronounced decrease in anisotropy seen in the later channels in the microscope data (Fig. 2 *b*) where the fura-2 fluorescence has decayed significantly, may be due to the larger relative contribution of background fluorescence in the microscope as compared with the cuvette data. In the microscope decays, the background fluorescence from an unlabeled cell is 5–10% of the labeled cell fluorescence at the peak of the decay, but increases to 20% in the later channels. For the decays measured in the cuvette instrument, the background is at least 10-fold lower. We have not identified the sources of all of the additional long-lived background in the microscope, but fluorescence and phosphorescence from the objective and coated glass in the optical train may contribute significantly.

The nanosecond fluorescence microscope is designed to measure the emission from a single cell. Because in many cases the number of fluorophores in the cell may be very low the instrument sensitivity was tested using DPH in mineral oil at several concentrations from 10 nM to 10 μM. DPH was chosen because of its high quantum yield and favorable absorption at 355 nm. The results indicated that the NFM can measure fluorescence lifetimes of DPH reproducibly at concentrations as low as 50 nM, but that the data become difficult to fit to the exponential model at 10–20 nM DPH due to the decreasing ratio of fluorescence to background. Fig. 3 illustrates the intensity (*a*) and anisotropy (*b*) decays of a 60-nM solution of DPH. From the analysis of the data τ_1 and τ_2 are 0.010 and 9.60 ns, f_2 = 0.999, $\langle\tau\rangle$ = 9.59 ns, and χ^2_R is 12.2. These results are similar to literature values for single exponential fits of DPH decays (9.54–9.7 ns) (32, 33). The fits of the series of DPH concentrations

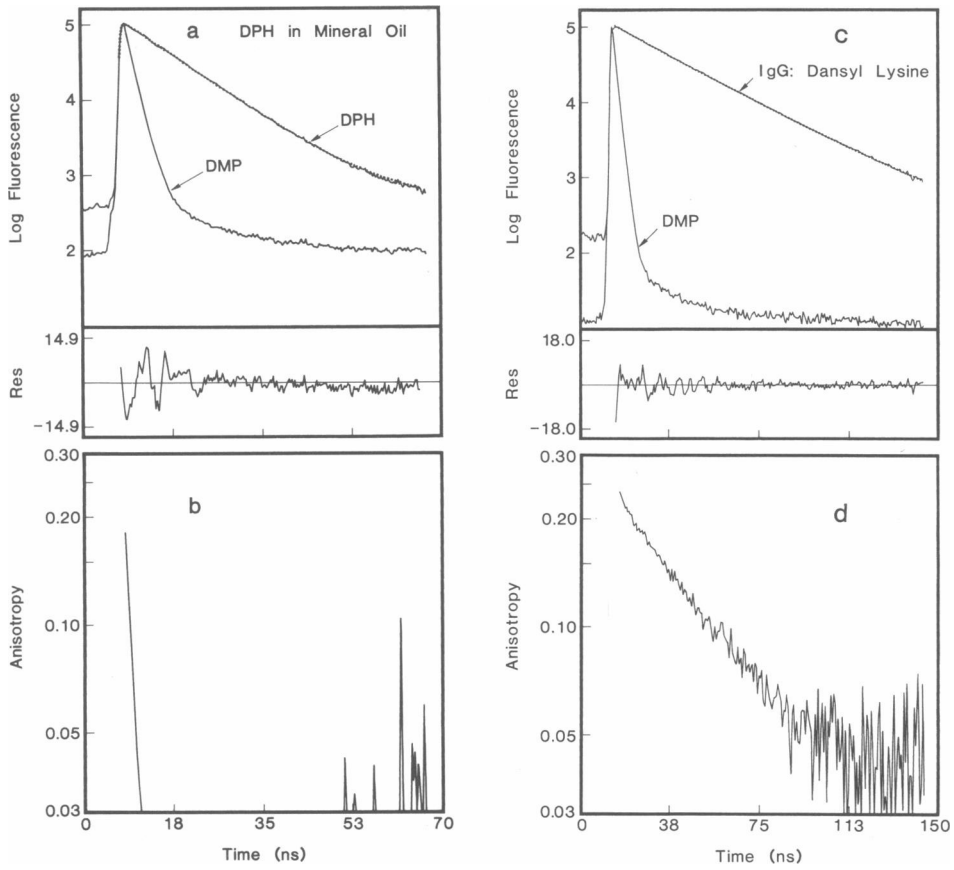

FIGURE 3 NFM Decays of DPH in mineral oil and of dansyllysine bound to IgG_{2b}. (*a*) The intensity decay of a 60 nM solution of DPH in mineral oil and DMP in ethanol measured in the nanosecond fluorescence microscope, with the weighted residuals from the fit. The data was fit over 165 channels. (*b*) The anisotropy decay of DPH in mineral oil. (*c*) The intensity decay of the dansyllysine bound to the combining site of IgG_{2b} (6 μM combining sites, 3 μM dansyllysine). The parameters for the lifetime fit shown (along with the weighted residuals) are $\tau_1 = 20.05$ ns, $\tau_2 = 28.81$ ns, $f_2 = 0.788$, $\chi^2 = 4.995$. (*d*) The anisotropy decay of dansyllysine bound to IgG_{2b}, measured in the NFM.

from 50 nM to 10 μM produce very similar results; the average lifetime is 9.61 ± 0.090 ns.

It is of interest to estimate the number of molecules the fluorescence is collected from under these conditions. To find the number of molecules in focus when collecting the decay from a 60-nM solution of DPH, we calculate the volume of solution in focus with the 1.30 NA objective. If the depth of field (DF) is described by (34),

$$DF = \lambda/[4n \sin^2(\sigma/2)], \tag{21}$$

where λ is the emission wavelength (0.450 μm), n is the refractive index of the medium containing the sample (for mineral oil, $n = 1.4673$), and σ is the half angle subtended by the objective (σ can be calculated from $NA = n \sin \sigma$), then $DF = 0.29$ μm. If we assume the volume in focus is a cylinder of radius 5.0×10^{-4} cm (from the diameter of the adjustable diaphragm) and height 2.9×10^{-5} cm, the volume is 2.3×10^{-11} cm^3 (or 23 fl). A 60-nM solution corresponds to 3.6×10^{13} molecules/cm^3, so that fluorescence is collected from 830 fluorophores. This calculation overestimates the number of observed fluorophores somewhat because it assumes that fluorescence is collected from the whole area imaged, while in fact the diameter of the excitation beam is smaller than the iris aperture, so that not all probes in the area are excited, and the number of in-focus molecules from which the emission is collected may be lower than estimated (by a factor of ~4 if the excitation covers only half the diameter of the image). However, fluorescence may also be collected from some out of focus dye molecules, compensating somewhat for the overestimation of in-focus molecules. Thus the calculation represents a fairly reliable upper limit of the number of DPH molecules required for accurate lifetime measurements under our experimental conditions. The minimum num-

ber of molecules required for accurate measurements in cells may be much higher because of interference from cell autofluorescence.

The anisotropy decay of the DPH sample is shown in Fig. 3 *b*. The anisotropy decay is rapid, as expected from the small size of DPH and from literature values of $\langle\phi\rangle$ of < 10 ns (32, 33) in slightly heavier grades of mineral oil. The apparent initial anisotropy (i.e., the maximal value observed in any time channel) is somewhat lower than values ($r_0 = 0.36$) measured in conventional instruments (32, 33). This discrepancy may be partly due to depolarization of both the excitation beam and the emitted light by the microscope optics, including the objective, and partly due to the inability of the instrument to resolve anisotropy decay components that are faster than the 156 ps time resolution of the TDC.

A better test of the instrument's capability for monitoring anisotropy decay kinetics is shown in Fig. 3 *d* where the anisotropy decay from dansyllysine bound to an antibody (mouse IgG_{2b}) is shown. The anisotropy kinetics of this probe bound to this antibody have been extensively studied (35, 36). The anisotropy decay curve is intermediate between those published in previous reports in which mean rotational correlation times of 47 ns (35) and 55 ns (36) were reported. The $\langle\tau\rangle$ value of 27 ns obtained from a double exponential fit of the intensity decay, shown in Fig. 3 *c*, is also close to the previously reported value of 26.5 ns (22) for antibody-bound dansyllysine.

Time-resolved anisotropy data measured in the microscope may be distorted by high NA effects described above (Data Analysis). To test for these effects, decays of DPH and fura-2 (salt) samples were measured with two objectives having the same magnification (100X) but different NA, 1.3 and 0.85 (data not shown). Analysis of the data revealed no difference between the intensity decays measured with the Neofluar (1.30 NA) and the Ultrafluar (0.85 NA) objectives within the experimental error of the measurements (±0.1 ns). However, the apparent values of the initial anisotropy for both probes were 14–25% lower when measured with the 1.3 NA objective than when measured with the 0.8 NA objective. As discussed above, the 1.30 NA objective may be expected to depolarize steady state data by as much as 25%. This depolarization may account for the somewhat lower apparent initial anisotropy observed in all the data measured in the microscope, as compared with the decays measured in the cuvette instrument. However, the kinetics of the anisotropy decays of these samples appear to be unaffected, in that the curves can be superimposed to within the experimental noise level by being shifted on the logarithmic scale. Because only the absolute value of the initial anisotropy appears to be affected by the numerical aperture, and not the decay kinetics, the data has not been corrected for high NA effects.

These experiments indicate that quality data can be reproducibly measured in the microscope, giving comparable lifetime data to the cuvette instrument. The significant difference is that these measurements can be made on 10^3 or fewer fluorophores. The anisotropy results are somewhat lower in quality than obtained from data measured in conventional instruments, with lower values of apparent initial anisotropy consistently obtained, and with loss of reliability in later channels when short lifetime probes are used (i.e., when $t > 3\ \langle\tau\rangle$). However the kinetics of the anisotropy decay, and therefore useful information about rotational diffusion, can be reliably monitored in the NFM for $t < 3\ \langle\tau\rangle$, yielding results that are similar to those obtained in conventional instruments.

Fura-2 lifetime measurements in the cuvette instrument

To determine whether the emission properties of fura-2 in cells are altered from those of the dye in solution, the intensity decays of the dye free in solution, protein-bound, and in cells were measured in the cuvette instrument and are shown together for comparison in Fig 4. The decays in Fig. 4 *a* are from fura-2 (salt form) with either EGTA or Ca^{2+} in buffer. The best double-exponential fit of the Ca^{2+} free fura-2 decay is shown by the dotted line through the data and described in Table 1. The decay has at least two components, and the average lifetime from the fit is 1.13 ns. With the addition of Ca^{2+} the lifetime increases and the decay becomes essentially single exponential, $f_2 = 0.911$ and $\tau_2 = 1.82$ ns; $\langle\tau\rangle = 1.71$ ns. The longer lifetime is consistent with the increase in quantum yield observed when Ca^{2+} binds to fura-2 (15). The fairly high values of χ^2_R obtained from some fits of the cuvette data appear to be partly due the presence of more than two lifetime components and partly due to inaccuracies in the instrument response function used for reconvolution. These inaccuracies primarily affect the fit in the early part of the decay and are largely eliminated in the deconvolution method used for the microscope data.

To determine what effect the high concentrations of protein found in cells might have on the fluorescence decays of fura-2, the decays of the salt form of the probe were measured in the presence of 32 mg/ml aldolase and 140 mM salt (Fig. 4 *b*). These conditions are similar to those previously shown to alter the apparent K_d for Ca^{2+} and cause spectral shifts (17). The decay of fura-2 in the presence of 25 mg/ml of creatine phosphokinase (CPK) and EGTA was also measured (CPK precipitates in Ca^{2+}). The proteins increase the mean lifetimes in the

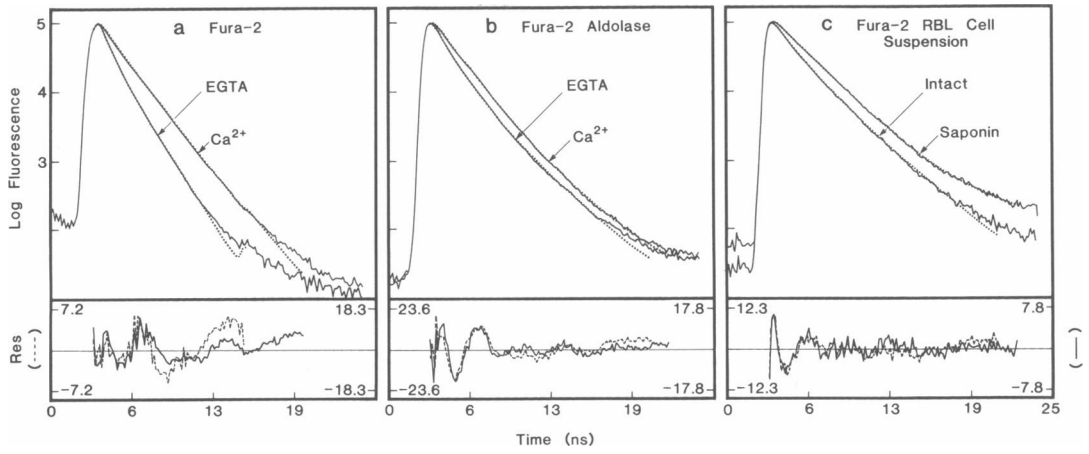

FIGURE 4 Comparison of free, protein-bound and intracellular Fura-2 intensity decays as measured in a cuvette. Samples shown as the solid lines, contain (*a*) fura-2 (salt) with either EGTA or Ca^{2+}, (*b*) fura-2 (salt) with aldolase and either EGTA or Ca^{2+}, and (*c*) intact and saponin permeabilized cell suspensions that had been loaded with fura-2 (ester). The dotted lines are the results of double-exponential fits of the data. In the bottom panels the weighted residuals from the fits of the data are shown. The Ca^{2+} data are the solid lines, the dashed lines the fits of the EGTA data; for (*c*) the solid lines are the fits of the permeabilized cell data, the dashed lines from the intact cell data analysis. The scales for the dashed lines are shown on the left and the solid lines on the right side of the panels. The fits of the decays are over 77 and 107 channels for fura-2 salt in EGTA and Ca^{2+}, respectively; fura-2 with protein, 113–123 channels; intact cells, 117 channels, permeabilized cells, 127 channels. All other conditions are as in Fig. 2.

presence of EGTA beyond the value observed for the free dye; $\langle\tau\rangle$ values shift to 1.58 ns (aldolase) and 2.04 ns (CPK). Aldolase had a less dramatic effect in the presence of Ca^{2+}.

To investigate the intracellular behavior of the dye, fluorescence decays from a solution of intact cells as well as from cells permeabilized with saponin were measured. The average lifetime from the fit of the data from the intact cells is 2.06 ns (Fig. 4 *c*). This is higher than the value of 1.71–1.88 ns observed for Ca^{2+}-saturated fura-2, and cannot be explained simply by binding to intracellular calcium. It is also unlikely to be due to unhydrolyzed ester, because (*a*) the absorbance peak for fura-2 loaded RBL cells is at 360 nm whereas the ester peak is ~400 nm, (*b*) the ester has a much lower fluorescence intensity than the free acid, and (*c*) the ester decay contains both very short (~1 ns) and much longer (~5 ns) lifetime components that are not observed in the cell data. The increase in lifetime observed in the loaded cells and protein solutions as compared with that of the dye in the simple buffer solutions indicates that fura-2 binds to proteins in solution and to unknown components within the cell, and that this binding influences its lifetime. The fluorescence decay from the intracellular dye is more complex than the double-exponential model used to fit the data, as evidenced by the nonrandomness of the weighted residual plots. This may result from the many different local environments in which the fluorophore exists in the cell, each of which may uniquely alter the decay kinetics.

The decay from a suspension of saponin-permeabilized cells is also shown in Fig 4 *c*. After permeabilization $\langle\tau\rangle$ increases to 2.62 ns. The lifetime increase upon permeabilization may be due to association with micelles containing saponin and cellular components that increase the dye's fluorescence lifetime, but do not restrict its rotational motion (as inferred from the rapid anisotropy decay, discussed below). Saponin alone (i.e., in the absence of cells) causes a slight increase in the lifetime of fura-2 ($\langle\tau\rangle$ increases ~0.2 ns, data not shown) but not enough to account for the increase observed here.

Fura-2 anisotropy measurements in the cuvette instrument

The anisotropy decays of fura-2 measured in the cuvette instrument for the same samples as in Fig. 4 are shown in Fig. 5. The results of fits of the data to a double-exponential decay law are shown as the dotted lines through the data and in Table 2. In the absence of protein, the fura-2 anisotropy decays in <1 ns, as expected for a small molecule (the rotational correlation time, ϕ, obtained from the fit of the data is 0.33 ns). However, the anisotropy decays of fura-2 in the presence of aldolase are nonexponential, with both fast ($\phi < 1$

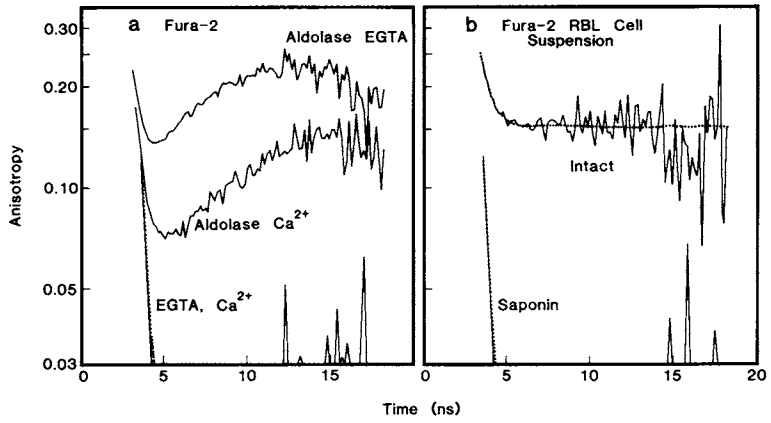

FIGURE 5 Comparison of free, protein-bound, and intracellular Fura-2 anisotropy decays - cuvette measurements. The anisotropy decays shown (—) are for the same samples as in Fig. 4. (*a*) Anisotropy data of free fura-2 in Ca^{2+} or EGTA, with or without aldolase. (*b*) The anisotropy decays from intact and saponin-permeabilized fura-2 loaded cells in suspension. The results of double-exponential fits of the data are also shown (···).

ns) and slow (ϕ > 100 ns) components. From inspection of the data, it is apparent that in the presence of EGTA and aldolase, the slower component is a larger fraction of the decay than when Ca^{2+} is included with aldolase. The data are obviously nonexponential and cannot be fit to a biexponential decay. Thus, correlation times from fits of the protein-fura-2 data are not included in Table 2. The presence of apparent decay components with a positive sign (i.e., the upward curvature of the decays) is consistent with a heterogenous population of emittors, in which species with long-lived intensity decays, as observed for the component lifetimes of fura-2 in the protein solutions shown in Table 2, are associated with the slower anisotropy components. This behavior was reproducibly observed in several measurements of fura-2 decays in aldolase and CPK. The nonexponential decays are probably not due to impurities introduced with the proteins because the protein solutions without fura-2 displayed negligible fluorescence at the wavelengths measured. The presence of EGTA minimizes the danger of interference from metal ions binding to fura-2 whereas salts and other small molecules are known to have only small effects of fura-2 fluorescence (18). Moreover, the high anisotropy values at long times after the pulse can only be caused by binding to something very large (i.e., a macromolecule). Thus, the results indicate that in the presence of high (i.e., comparable to intracellular) protein concentrations, fura-2 is complexed with the proteins, in agreement with the results of Konishi et al. (17).

TABLE 2 Fits of time-resolved anisotropy decays of Fura-2

Conditions	β_1*	ϕ_1	β_2	ϕ_2	χ^2_R
		ns		*ns*	
Ca^{2+}	0.0265	0.314	0.317	0.314	16.3
EGTA	0.0137	0.333	0.331	0.333	4.61
RBL cells, intact	0.246	0.453	0.154	1260	1.77
RBL cells, saponin	0.399	0.354	0.0408	0.353	1.41

*All decays were analyzed using a double-exponential fit.

The anisotropy decays recorded from suspended intact RBL cells loaded with fura-2 (Fig. 5 *b*) also contain a slowly decaying component with a high limiting anisotropy. These data indicate that a significant fraction of the dye molecules in the cell must be bound to macromolecules or supramolecular structures of high molecular weight. The fit of the data gives ϕ_1 = 0.453 ns, β_1 = 0.246, ϕ_2 = 1260 ns, and β_2 = 0.154 (Table 2). It is unlikely that light scattering is the primary cause of the high initial anisotropy values observed in the high protein and cell systems because only very weak signals are detected from samples without the dye and because the decays did not have the sharp initial spike in the intensity decays that is observed in strongly scattering samples. Furthermore, interference due to scattering of the excitation pulse cannot occur past the ~600 ps instrument response time.

When the cells are permeabilized with saponin, fura-2 again displays the rapid anisotropy decay characteristic of a small molecule (ϕ = 0.30 ns) (Fig. 5 *b*). While the dye is not truly free in solution under these conditions, as indicated by the enhanced fluorescence lifetime, the dramatic change in the anisotropy decay upon saponin treatment indicates that in intact cells (*a*) the immobile fraction of fura-2 is probably within the cytosol and not localized within organelles (at least not in ones that are inaccessible to saponin) and (*b*) its binding to large

cellular components is noncovalent, reversible, and relatively weak.

Fura-2 lifetime measurements in the NFM

The measurements of the suspension of loaded cells are an average of the decays of fura-2 in all the cells illuminated. It is unclear whether in some cells fura-2 is in the free, uncomplexed form and in others bound to macromolecules, or whether the dye is bound in all cells. Therefore, the time-resolved decays of fura-2 were also measured in the nanosecond fluorescence microscope where the decays from individual cells can be separately collected to determine the environmental properties of the intracellular dye. The decay of the free dye in solutions similar to those measured in the cuvette pulse instrument were also recorded for comparison (Fig. 6). In the presence of EGTA the mean lifetime is 1.25 ns whereas in Ca^{2+} the decay is again essentially a single exponential, with τ = 1.88 ns. Under the present experimental conditions and analysis procedures a biexponential result with the components differing by 4% cannot be distinguished from a single component result. These results are similar to those obtained with the cuvette instrument.

Figs. 2 *b* and 6, *b* and *c* illustrate the fluorescence decays of fura-2 in single adherent cells loaded via the ester. In the cells the average lifetime increases to 1.92–1.97 ns, slightly longer than that of Ca^{2+}-saturated fura-2, as found in the cell suspension ($\langle\tau\rangle$ = 2.06 ns). All the decays are multiexponential, with the lifetime components from the double exponential fits consistently differing by at least a factor of two. Cell 1 was loaded with 2.5 μM fura-2 for 45 min whereas cells 2 and 3 (on different areas of the same slide) were labeled for 30 min with 1 μM fura-2. During the measurements the intensity (i.e., the count rate) did not significantly decrease over 10–15 min, indicating that leakage of the dye from the cell and photobleaching are not significant problems. Whenever a second decay was recorded from a cell, virtually identical intensity and anisotropy decays were obtained both times. Thus, cell movements on the time scale of the measurements do not seem to affect the results significantly.

Fura-2 anisotropy measurements in the NFM

The NFM anisotropy decays from these cells are shown in Figs. 2 *b* and 7, and decays from fura-2 in solution, with or without Ca^{2+} bound are shown in Fig. 7 *a*. The rapid anisotropy decays of the free dye are very similar to those observed in the cuvette. The decay of the dye in the single cells contain the fast and slow components seen in the suspended cells. However, comparison of the decays from the three cells indicates that the contribution of the fast component is different in each cell. In all cells examined, the anisotropy displayed both the fast and slow components exhibited in Fig. 7, indicating that fura-2 is bound to macromolecules in all these cells. The

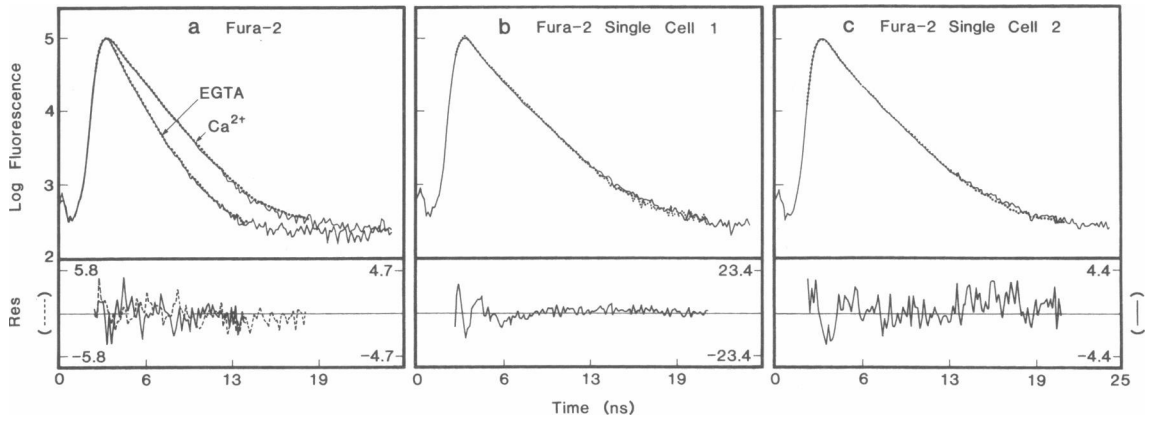

FIGURE 6 Intensity decays of free and intracellular Fura-2 measured in the microscope. The time-resolved intensity decays of fura-2 were measured in the nanosecond fluorescence microscope (*solid lines*). (*a*) Fura-2 (salt) in buffer, in the presence of Ca^{2+} or EGTA. (*b*) The decay of a single RBL cell loaded with fura-2 (cell 1). (*c*) A different cell, loaded under different conditions than the cell in *b* (cell 2). The results of fits of the data to a double-exponential model (*dotted lines*) are also shown with the weighted residuals in the bottom panel. The scale for the dashed lines is on the left side and the solid lines on the right side of the panel. In *a*, the residuals shown as the dashed lines are from the fit of the Ca^{2+} data; the solid lines are from the fit of the EGTA data. (*a*) Data fit was over 72 and 102 channels for EGTA and Ca^{2+}, respectively; (*b*, *c*) Fit over 122 channels. All other conditions were as in Fig. 2.

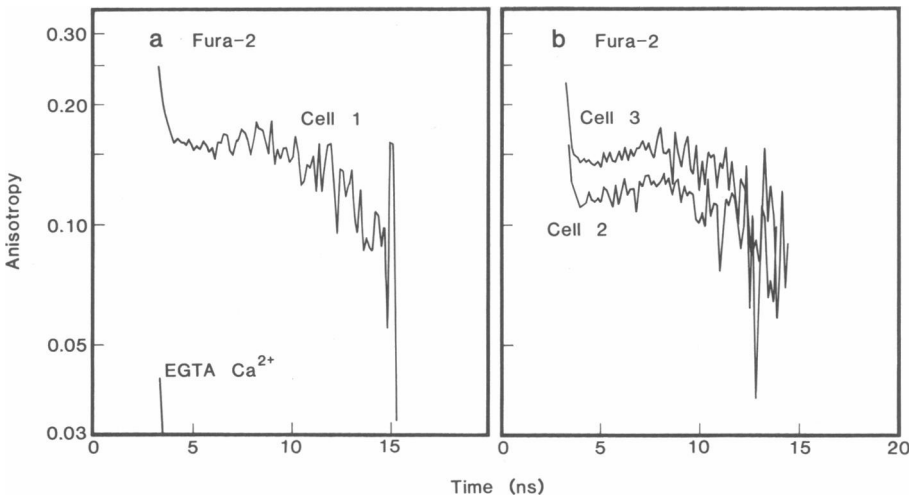

FIGURE 7 Anisotropy decays of free and intracellular Fura-2 measured in the microscope. Anisotropy decays are shown for the same samples as in Fig. 6. Decays of free fura-2, with or without Ca^{2+} bound and in cell 1 are shown in *a;* decays from two cells labeled together but under different conditions than cell 1 are shown in *b.* The decay of cell 3 in *b* is the same as that in Fig 2 *b.* Other conditions were as in Fig. 6.

variation in the relative amplitudes of each component from cell to cell indicates that the dye is not in an identical environment, even in cells labeled under identical conditions (compare the decays from cells 2 and 3, Fig. 7 *b*). Measurements of an additional number of cells (over 30) under a variety of conditions confirmed that the cell-to-cell variability is a general phenomenon. While the data may be subject to some uncertainty due to scattering during the first 600 ps, and due to background in the later (more than 6 ns after the pulse) channels, the evidence for slowly decaying anisotropy and cell-to-cell variation is primarily provided by the intermediate channels containing the most reliable anisotropy data.

Fura-2 spectral shifts

The excitation and emission spectra of fura-2 were measured under the same conditions as those used to measure the excited state decays (data not shown). While the observed spectral shifts of the free dye when it binds Ca^{2+} concur with literature values (15), we found that the excitation and emission spectra were modified in the presence of proteins or in cells, with the intracellular data showing the greatest deviations from the spectra of simple buffer solutions. The intracellular emission spectrum of fura-2 is blue-shifted from that of the free dye ($\pm Ca^{2+}$) at least 8 nm, while the excitation spectra of the dye in cells are intermediate between those for the free dye with and without Ca^{2+}. The excitation spectra in the aldolase solutions are close to those of the free dye, but the emission spectra are intermediate between those observed for the Ca^{2+}-free dye and for Ca^{2+}-saturated dye.

CONCLUSIONS

Our results demonstrate that the intensity and anisotropy decay kinetics of fluorescent probes can be readily measured on the nanosecond time scale in single cells. The NFM instrument described here can be used to obtain reliable data from samples in which $\sim 10^3$ fluorophores are emitting. The data are comparable among separate sample preparations and are similar to those obtained from populations of cells in suspension. However, the single cell studies show variations from cell to cell that are not possible to detect in cuvette measurements. It is worth noting that the microscope is not as sensitive as is possible with current technology. This instrument is built around a Carl Zeiss Inc. Universal microscope which contains more coated glass in the emission train than later models, reducing the intensity of transmitted light $\sim 25\%$ at each interface. Thus, more sensitive microscope-based single photon counting instruments can be constructed.

The analysis of the data used here is fairly simplified; only double-exponential models were used to fit the data. Although the intracellular decays are more complex than double exponentials, useful information can be obtained by comparing the best fit lifetimes and the qualitative features of the depolarization kinetics. No attempt has been made to calculate double exponential fits for the intracellular anisotropy kinetics as they

deviate greatly from exponential behavior, and also obviously contain components that are much longer than 12 ns and therefore cannot be accurately measured with a probe having a 2-ns excited-state lifetime. The raw anisotropy data has been presented because they clearly demonstrate the altered rotational behavior of a substantial portion of the dye. If we were to assume that there are two populations of dye, bound and free, each characterized by a biexponential intensity decay and biexponential anisotropy decay, it should be possible, in principle, to obtain by fitting the data to such a model, the fraction of bound dye and its rotational correlation time. We have not attempted such fits for two reasons: (*a*) such modeling would require a 14 parameter fit, which is not warranted by the quality of this data; (*b*) it seems unlikely that there are actually only two populations of dye in the cell.

In addition to the high NA effects already discussed, more trivial causes of depolarization (such as laser beam scattering in the microscope and any depolarization effects of the dichroic mirror) may lead to further reductions in the anisotropy values measured in the microscope. However, these effects are primarily on the absolute values of the anisotropy rather than on the kinetics and should not alter the interpretation of the decays reported here. In general the highest value of anisotropy observed in the beginning of the decay, which we treat as the apparent initial anisotropy, cannot be assumed to reflect the true initial, or limiting anisotropy. In fact, the true initial anisotropy, which is essentially a function of the angle between the absorption and emission transition dipoles, and the wavelength, probably does not change much from sample to sample for a given dye. Low apparent values may reflect either artifactual depolarizing effects, or components whose decay is too fast to be monitored within the instrument's time resolution.

The time-resolved fluorescence data at high protein concentrations confirm that fura-2 does in fact bind to proteins in solution, resulting in markedly changed emission anisotropy and intensity decays. Fura-2 has in fact been reported to bind weakly to proteins; probably through electrostatic interactions as the binding is somewhat dependent on ionic strength (17). Similar effects are observed in cells, and can only be explained by fura-2 binding to high molecular weight components. That the intracellular excited state emission is modified from that observed in simple buffer solutions is also demonstrated by the altered spectra observed in protein solutions and loaded cells reported by others (17) and observed in our measurements. It is not surprising that the more complex (and probably more hydrophobic) environments interfere with the spectral shifts of the dye observed with changes in Ca^{2+} concentrations in simple buffer solutions. That the emission of the intracellular form of the probe is modified more than that of fura-2 in protein solutions is also not unexpected, considering the more complex intracellular environment.

Some of the known problems associated with use of fura-2 are incomplete ester hydrolysis, compartmentization of the dye into organelles, and extrusion of the dye by anion transport mechanisms (18). We have seen no evidence for these phenomenon under our conditions. As explained above (Results) it is unlikely that any unhydrolyzed ester that may be present in the cells contributes significantly to the signal. The cells were loaded at 23° and not at 37°C, because at 37° compartmentation of dye (18, 37) leakage, and redistribution of fura-2 in RBL cells are known to occur (38). Extrusion of the dye does not seem to be a problem, as indicated by the constant signal level over the time course of the experiment. The fact that all the dye displaying hindered rotation is accessible to saponin permeabilization means that any fura-2 containing organelles in RBL cells, unlike those containing IP_3-gated Ca^{2+} channels and the Ca^{2+}-ATPase (39), would have to be permeabilized by saponin. When RBL cells are labeled at 37°C, there is clearly compartmentation, as indicated by dark spots of concentrated dye. These spots were not observed in cells labeled at 23°C when a 40X or 100X objective was focused on the cell and the plane of focus moved up and down through the cell. In the time-resolved measurements we do not image the cell, but collect one emission signal from the whole cell; thus this data also does not contain information concerning local distribution of the dye. Thus, while compartmentalization cannot be ruled out, we can conclude that if it is present (*a*) either the compartments are very small or have fura-2 concentrations not very different from the average throughout the cell; (*b*) these compartments are permeabilized by saponin; (*c*) similar compartmentation would likely be present in the many cells whose Ca^{2+} levels have been monitored using fura-2 loaded under similar conditions.

In the future NFM measurements may provide unique information about the environment and mobility of probes in their physiological setting. In addition, this technique should prove valuable for samples where the background fluorescence and scatter from cell suspensions leads to unsatisfactory signal-to-noise ratios, in cases where a substrate for cell adhesion is needed, or when sample quantity is limiting. Furthermore, this method may be developed to include the measurement of spatial as well as temporal information; i.e., the collection of time-resolved decays at different points in an imaged cell. NFM energy transfer as well as depolarization measurements may prove useful for structural

studies of cell surface as well as intracellular molecules, including components involved in receptor-ligand and protein-lipid interactions.

APPENDIX

Models for analysis of time resolved data

We describe the models used for analysis of data using a reference because in contrast to the well-known procedures for analysis of time-correlated single photon data using a scatterer (4, 23), the analysis of data using a reference employed in this study is less commonly used. The measured fluorescence response, $F_S(t)$, of the sample to the pulsed excitation is a convolution of the true fluorescence decay of the sample, $f_S(t)$, and the instrument response, $I(t, \lambda_{ex}, \lambda_{em})$.

$$F_S(t, \lambda_{ex}, \lambda_{em}) = I(t, \lambda_{ex}, \lambda_{em}) * f_S(t), \quad \text{(A1)}$$

where the subscript S refers to the sample and λ_{ex} and λ_{em} are the excitation and emission wavelengths. In the usual analysis of time-resolved data and the procedure we use for analysis of data measured in the cuvette instrument, $f_S(t)$ is calculated using a model to approximate the true decay and convolved with the measured instrument response to fit $F_S(t)$. The model we use to fit the data is the response of a sum of exponentials to a Dirac δ-excitation function:

$$f_S(t) = \Sigma_i \alpha_i e^{-t/\tau_i}, \quad \text{(A2)}$$

where α_i is the amplitude and τ_i the lifetime of component *i*. A double-exponential model is used in all the fits, which assumes that the probe experiences at least two different environments or exists in two different states during the excited-state lifetime. The true instrument response profile is itself the convolution of the time profile of the pulse at the excitation wavelength, $L(t, \lambda_{ex})$ and the response of the instrument electronics at the emission wavelength, $R(t, \lambda_{em})$,

$$I(t, \lambda_{ex}, \lambda_{em}) = L(t, \lambda_{ex}) * R(t, \lambda_{em}). \quad \text{(A3)}$$

However, because $I(t)$ is usually measured using a scatter at λ_{ex}, an approximation of the instrument response function is actually used in the convolution:

$$I(t, \lambda_{ex}, \lambda_{ex}) = L(t, \lambda_{ex}) * R(t, \lambda_{ex}). \quad \text{(A4)}$$

The use of a reference for the analysis of pulse data has been discussed by several authors (24, 25, 40–43) as a method to account more accurately for photomultiplier "color effects", in which the transit time of photoelectrons through the photomultiplier can vary depending on the wavelength of light impinging on the photocathode (44). In the "delta function deconvolution" method used in the analysis of the microscope data, the decay of a reference, $F_R(t, \lambda_{ex}, \lambda_{em})$, with a known, single exponential lifetime, τ_R, is measured at the same excitation and emission wavelengths as that of the sample, $F_S(t, \lambda_{ex}, \lambda_{em})$. Recall Eq. A1. Then

$$F_R(t, \lambda_{ex}, \lambda_{em}) = I(t, \lambda_{ex}, \lambda_{em}) * f_R(t), \quad \text{(A5)}$$

where

$$f_R(t) = \alpha_R e^{-t/\tau_R}. \quad \text{(A6)}$$

The subscript R refers to the reference. In the fitting routine, the sample response is fit to an altered model for the sample decay, $f'_S(t)$,

$$F_S(t, \lambda_{ex}, \lambda_{em}) = I(t, \lambda_{ex}, \lambda_{em}) * f_R(t) * f'_S(t) \quad \text{(A7)}$$

or,

$$F_S(t, \lambda_{ex}, \lambda_{em}) = F_R(t, \lambda_{ex}, \lambda_{em}) * f'_S(t). \quad \text{(A8)}$$

$f'_S(t)$ is modeled as a sum of exponentials,

$$f'_S(t) = \Sigma_i \alpha_i[\delta_0(t) + (1/\tau_R - 1/\tau_i)e^{-t/\tau_i}], \quad \text{(A9)}$$

where $\delta_0(t)$ is the Dirac delta function at time 0. Thus,

$$F_S(t, \lambda_{ex}, \lambda_{em}) = \Sigma_i \alpha_i * F_R(t, \lambda_{ex}, \lambda_{em}) + F_R(t, \lambda_{ex}, \lambda_{em}) * [\Sigma_i \alpha_i(1/\tau_R - 1/\tau_i)e^{-t/\tau_i}]. \quad \text{(A10)}$$

The anisotropy decay of a fluorophore is a measure of the randomization of the excited state chromophores by rotational Brownian motion after excitation by polarized light. The kinetics of randomization depend on the size and shape of the probe, whether it is free in solution or bound to another molecule. If bound to a macromolecule, the anisotropy decay will be dependent on the size and shape of the macromolecule as well as the flexibility of the region bound to the fluorophore. The anisotropy, $r_S(t)$, is defined as:

$$r_S(t) = [f_V(t) - f_H(t)]/[f_V(t) + 2f_H(t)], \quad \text{(A11)}$$

where f_V and f_H are the parallel and perpendicular components of the true decay. To fit the data a double exponential is again used to model the decay;

$$r_S(t) = \Sigma_i \beta_i e^{-t/\phi_i}, \quad \text{(A12)}$$

where β_i is the amplitude and ϕ_i is the rotational correlation time of component *i*.

In the analysis of the data the lifetimes and rotational correlational times are not associated (2).

The authors wish to thank Drs. J. B. A. Ross and W. Laws for help with the data analysis, Drs. T. Meyer and S. Kron for their generous advice, as well as Dr. Aaron B. Kantor for providing anti-dansyl IgG_{2b}, and William Magni for machining of parts. We are especially grateful for the encouragement of Prof. L. Stryer in whose laboratory this work was done.

This work was supported by National Institutes of Health fellowships AR07803 to Dr. Keating and EY05815 to Dr. Wensel and by grant GM24032 to Dr. L. Stryer.

Received for publication 30 November 1989 and in final form 16 July 1990.

REFERENCES

1. Lakowicz, J. R. 1983. Principles of Fluorescence Spectroscopy. Plenum Press, New York. 496 pp.
2. Brand L., J. R. Knutson, L. Davenport, J. M. Beechem, R. E. Dale, D. G. Walbridge, and A. A. Kowalczyk. 1985. Time-resolved

fluorescence spectroscopy: some applications of associative behaviour to studies of proteins and membranes. *In* Spectroscopy and the Dynamics of Molecular Biological Systems. P. M. Bayley and R. E. Dale, editors. Academic Press, Inc., London. 259–305.

3. Beechem, J. M., and L. Brand. 1985. Time-resolved fluorescence of proteins. *Annu. Rev. Biochem.* 54:43–71.
4. O'Connor, D. V., and D. Phillips. 1984. Time-Correlated Single Photon Counting. Academic Press, Inc., London. 288 pp.
5. Gratton, E., M. Limkeman, J. R. Lakowicz, B. P. Maliwal, H. Cherek, and G. Laczko. 1984. Resolution of mixtures of fluorophores using variable-frequency phase and modulation data. *Biophys J.* 46:479–486.
6. Lakowicz, J. R., G. Laczko, and I. Gryczynski. 1987. Picosecond resolution of tyrosine fluorescence and anisotropy decays by 2-GHz frequency-domain fluorometry. *Biochemistry.* 26:82–90.
7. Koppel, D. E., D. Axelrod, J. Schlessinger, E. I. Elson, and W. W. Webb. 1976. Dynamics of fluorescence markers concentrations as a probe of motility. *Biophys. J.* 16:1315–1329.
8. Yoshida, T. M., and B. G. Barisas. 1986. Protein rotational motion in solution measured by polarized fluorescence depletion. *Biophys. J.* 50:41–53.
9. Velez, M., and D. Axelrod. 1988. Polarized fluorescence photobleaching recovery for measuring rotational diffusion in solutions and membranes. *Biophys. J.* 53:575–591.
10. Docchio, F., R. Ramponi, C. A. Sacchi, G. Bottiroli, and I. Freitas. 1984. An automatic pulsed laser microfluorometer with high spatial and temporal resolution. *J. Microsc.* 134:151–160.
11. Pleil, M. W., S. Gangopadhyay, and W. L. Borst. 1987. Primary scintillant fluorescence decay times in binary and ternary scintillators by near UV pulsed laser excitation. *Nucl. Instr. Methods Phys. Res.* A256:348–354.
12. Murray, J. G., R. B. Cundall, C. G. Morgan, G. B. Evans, and C. Lewis. 1986. A single-photon-counting fourier transform microfluorometer. *J. Phys. E: Sci. Instrum.* 19:349–355.
13. Rogers, M. A. J., and P. A. Firey. 1985. Instrumentation for fluorescence microscopy with picosecond time resolution. *Photochem. Photobiol.* 42:613–616.
14. Kusumi, A., A. Tsuji, M. Murata, Y. Sako, A. Yoshizawa, T. Hayakawa, and S. Ohnishi. 1988. Development of a time-resolved microfluorimeter with a synchroscoan streak camera and its application to studies of cell membranes. *In* SPIE Proceedings. 909. J. R. Lakowicz, editor. 350–351.
15. Grynkiewicz, G., M. Poenie, and R. Y. Tsien. 1985. A new generation of Ca^{2+} indicators with greatly improved fluorescence properties. *J. Biol. Chem.* 260:3440–3450.
16. Baylor, S. M., and S. Hollingsworth. 1988. Fura-2 calcium transients in frog skeletal muscle fibres. *J. Physiol.* 403:151–192.
17. Konishi, M., A. Olson, S. Hollingworth, and S. M. Baylor. 1988. Myoplasmic binding of fura-2 investigated by steady-state fluorescence and absorbance measurements. *Biophys J.* 54:1089–1104.
18. Tsien, R. Y. 1989. Fluorescent indicators of ion concentrations. *In* Methods in Cell Biology. 30. D. L. Taylor and Y. Wang, editors. Academic Press, Inc., San Diego, CA. 127–156.
19. Wassler, M., I. Jonasson, R. Persson, and E. Fries. 1987. Differential permeabilization of membranes by saponin treatment of isolated rat hepatocytes. Release of secretory proteins. *Biochem. J.* 247:407–415.
20. Millard, P. J., D. Gross, W. W. Webb, and C. Fewtrell. 1988. Imaging asynchronous changes in intracellular Ca^{2+} in individual stimulated tumor mast cells. *Proc. Natl. Acad. Sci. USA.* 85:1854–1858.
21. Reidler, J., V. T. Oi, W. Carlsen, T. M. Vuong, I. Pecht, L. A. Herzenberg, and L. Stryer. 1982. Rotational dynamics of monoclonal anti-dansyl antibodies. *J. Mol. Biol.* 158:739–746.
22. Wensel, T. G., W. P. Schneider, V. T. Oi, and L. Stryer. 1989. Nanosecond motions of genetically engineered antibodies: structural elements controlling segmental flexibility defined by time-resolved emission anisotropy. *In* SPIE Proceedings. 909. J. R. Lakowicz, editor. 108–112.
23. Grinvald, A., and I. Z. Steinberg. 1974. On the analysis of fluorescence decay kinetics by the method of least-squares. *Anal. Biochem.* 59:583–598.
24. Zuker, M., A. G. Szabo, L. Bramall, D. T. Krajcarski, and B. Selinger. 1985. Delta function convolution method (DFCM) for fluorescence decay experiments. *Rev. Sci. Instrum.* 56:14–22.
25. Lofroth, J. E. 1985. Deconvolution of single photon counting data with a reference method and global analysis. *Eur. Biophys. J.* 13:45–58.
26. Marquardt, D. W. 1963. An algorithm for least-squares estimation of nonlinear parameters. *J. Soc. Indust. Appl. Math.* 11:431–441.
27. Bevington, P. R. 1969. Data Reduction and Error Analysis for the Physical Sciences. McGraw-Hill, New York. 336 pp.
28. Wahl, Ph. 1979. Analysis of fluorescence aniostropy decays by a least square method. *Biophys. Chem.* 10:91–104.
29. Axelrod, D. 1979. Carbocyanine dye orientation in red cell membrane studied by microscopic fluorescence polarization. *Biophys. J.* 26:557–573.
30. Axelrod, D. 1989. Fluorescence polarization microscopy. *In* Methods in Cell Biology. 30. D. L. Taylor and Y. Wang, editors. Academic Press, Inc., San Diego, CA. 333–352.
31. Lakowicz, J. R., H. Cherek, and A. Balter. 1981. Correction of timing errors in photomultiplier tubes used in phase-modulation fluorometry. *J. Biochem. Biophys. Methods.* 5:131–146.
32. Kawato, S., K. Kinosita, Jr., and A. Ikegami. 1977. Dynamic structure of lipid bilayers studied by nanosecond fluorescence techniques. *Biochemistry.* 16:2319–2324.
33. Dale, R., L. A. Chen, and L. Brand. 1977. Rotational relaxation of the "microviscosity" probe diphenylhexatriene in paraffin oil and egg lecithin vesicles. *J. Biol. Chem.* 252:7500–7510.
34. Inoue, S. 1986. Video Microscopy. Plenum Press, New York. 584 pp.
35. Oi, V. T., T. M. Vuong, R. Hardy, J. Reidler, J. Dangl, L. A. Herzenberg, and L. Stryer. 1983. Correlation between segmental flexibility and effector function of antibodies. *Nature (Lond.).* 307:136–140.
36. Dangl, J. L., T. W. Wensel, S. L. Morrison, L. Stryer, L. A. Herzenberg, and V. T. Oi. 1988. Segmental flexibility and complement fixation of genetically engineered chimeric human, rabbit, and mouse antibodies. *EMBO (Eur. Mol. Biol. Organ.) J.* 7:1989–1994.
37. Al-Mohanna, F. A., and M. B. Hallett. 1988. The use of fura-2 to determine the relationship between cytoplasmic free Ca^{2+} and oxidase activation in rat neutrophils. *Cell Calcium.* 9:17–26.
38. Millard, P. J., T. A. Ryan, W. W. Webb, and C. Fewtrell. 1989. Immunoglobulin E receptor cross-linking induces oscillations in intracellular free ionized calcium in individual tumor mast cells. *J. Biol. Chem.* 264:19730–19739.

39. Meyer, T., D. Holowka, and L. Stryer. 1988. Highly cooperative opening of calcium channels by inositol 1,4,5-triphosphate. *Science (Wash. DC).* 240:653–656.

40. Wahl, Ph., J. C. Auchet, and B. Donzel. 1974. The wavelength dependence of the response of a pulse fluorometer using the single photoelectron counting method. *Rev. Sci. Instrum.* 45:28–32.

41. Libertini, L. J., and E. W. Small. 1984. F/F deconvolution of fluorescence decay data. *Anal. Biochem.* 138:314–318.

42. Kolber, Z. S., and M. D. Barkely. 1986. Comparison of approaches to the instrumental response function in fluorescence decay measurements. *Anal. Biochem.* 152:6–21.

43. Vos, K., A. van Hoek, and A. J. W. Visser. 1987. Application of a reference convolution method to tryptophan fluorescence in proteins. *Eur. J. Biochem.* 165:55–63.

44. Lewis, C., W. R. Ware, L. J. Doemeny, and T. L. Nemzek. 1973. The measurement of short-lived fluorescence decays using the single photon counting method. *Rev. Sci. Instrum.* 44:107–114.